Research Article | Vol. 8, No. 3 | 1 Mar 2018 | OPTICAL MATERIALS EXPRESS 555
Optical Materials EXPRESS

Performance characterization of mid-infrared difference-frequency-generation in orientation-patterned gallium phosphide

JUNXIONG WEI,[1] S. CHAITANYA KUMAR,[1,2,*] HANYU YE,[1] P. G. SCHUNEMANN,[3] AND M. EBRAHIM-ZADEH[1,2,4]

[1]*ICFO-Institut de Ciencies Fotoniques, The Barcelona Institute of Science and Technology, 08860 Castelldefels (Barcelona), Spain*
[2]*Radiantis, Polígon Camí Ral, 08850 Gavà, Barcelona, Spain*
[3]*BAE Systems Incorporated, MER15-1813, P.O. Box 868, Nashua, NH 03061-0868, USA*
[4]*Institucio Catalana de Recerca i Estudis Avancats (ICREA), Passeig Lluis Companys 23, Barcelona 08010, Spain*
**chaitanya.suddapalli@radiantis.com*

Abstract: We present a detailed characterization of the optical properties of the recently developed nonlinear material, orientation-patterned gallium phosphide (OP-GaP), by performing difference-frequency-generation experiments in the 2548-2782 nm wavelength range in the mid-infrared (mid-IR). Temperature and spectral acceptance bandwidth measurements have been performed to study the phase-matching characteristics of OP-GaP, and the dependence of nonlinear gain on the polarization of input incident fields has been investigated. The transmission of the OP-GaP crystal at the pump and signal wavelengths has been studied and found to be dependent on polarization as well as temperature. Further, we have observed a polarization-dependent spatial shift in the transmitted pump beam through the OP-GaP sample. We have also measured the damage threshold of the OP-GaP crystal to be 0.84 J/cm^2 at 1064 nm.

OCIS codes: (190.4400) Nonlinear optics, materials; (190.4360) Nonlinear optics, devices; (190.4410) Nonlinear optics, parametric processes

References and links

1. M. W. Sigrist, "Mid-infrared laser-spectroscopic sensing of chemical species," J. Adv. Res. **6**(3), 529–533 (2015).
2. V. A. Serebryakov, É. V. Boĭko, N. N. Petrishchev, and A. V. Yan, "Medical applications of mid-IR lasers. Problems and prospects," J. Opt. Technol. **77**(1), 6–17 (2010).
3. M. Ebrahim-Zadeh and I. T. Sorokina, Mid-Infrared Coherent Sources and Applications, New York, NY, USA: Springer, 2008.
4. M. Ebrahim-Zadeh and K. Vodopyanov, "Mid-infrared coherent sources and applications: introduction," J. Opt. Soc. Am. B **33**(11), MIC1 (2016).
5. S. D. Jackson, "Towards high-power mid-infrared emission from a fibre laser," Nat. Photonics **6**(7), 423–431 (2012).
6. Y. Yao, A. J. Hoffman, and C. Gmachl, "Mid-infrared quantum cascade lasers," Nat. Photonics **6**(7), 432–439 (2012).
7. R. Bhatt, I. Bhaumik, S. Ganesamoorthy, R. Bright, M. Soharab, A. K. Karnal, and P. K. Gupta, "Control of intrinsic defects in lithium niobate single crystals for optoelectronic applications," Crystals **7**(2), 23 (2017).
8. M. Henriksson, M. Tiihonen, V. Pasiskevicius, and F. Laurell, "Mid-infrared ZGP OPO pumped by near-degenerate narrowband type-I PPKTP parametric oscillator," Appl. Phys. B **88**(1), 37–41 (2007).
9. R. K. Feaver, R. D. Peterson, and P. E. Powers, "Longwave-IR optical parametric oscillator in orientation-patterned GaAs pumped by a 2 µm Tm,Ho:YLF laser," Opt. Express **21**(13), 16104–16110 (2013).
10. K. Devi, P. G. Schunemann, and M. Ebrahim-Zadeh, "Continuous-wave, multimilliwatt, mid-infrared source tunable across 6.4-7.5 µm based on orientation-patterned GaAs," Opt. Lett. **39**(23), 6751–6754 (2014).
11. V. Petrov, "Parametric down-conversion devices: The coverage of the mid-infrared spectral range by solid-state laser sources," Opt. Mater. **34**(3), 536–554 (2012).
12. V. Petrov, "Frequency down-conversion of solid-state laser sources to the mid-infrared spectral range using non-oxide nonlinear crystals," Prog. Quantum Electron. **42**, 1–106 (2015).

#314757 https://doi.org/10.1364/OME.8.000555
Journal © 2018 Received 1 Dec 2017; revised 23 Jan 2018; accepted 30 Jan 2018; published 8 Feb 2018

Optical Materials EXPRESS

13. P. G. Schunemann, K. T. Zawilski, L. A. Pomeranz, D. J. Creeden, and P. A. Budni, "Advances in nonlinear optical crystals for mid-infrared coherent sources," J. Opt. Soc. Am. B **33**(11), D36–D43 (2016).
14. L. A. Pomeranz, P. G. Schunemann, D. J. Magarrell, J. C. McCarthy, K. T. Zawilski, and D. E. Zelmon, "1-μm-pumped OPO based on orientation-patterned GaP," Proc. SPIE **9347**, 93470K (2015).
15. P. G. Schunemann, L. A. Pomeranz, and D. J. Magarrell, "First OPO based on orientation-patterned gallium phosphide (OP-GaP)," in CLEO: Science and Innovations (Optical Society of America, 2015), paper SW3O–1.
16. J. Wei, S. Chaitanya Kumar, H. Ye, K. Devi, P. G. Schunemann, and M. Ebrahim-Zadeh, "Nanosecond difference-frequency generation in orientation-patterned gallium phosphide," Opt. Lett. **42**(11), 2193–2196 (2017).
17. H. Ye, S. Chaitanya Kumar, J. Wei, P. G. Schunemann, and M. Ebrahim-Zadeh, "Optical parametric generation in orientation-patterned gallium phosphide," Opt. Lett. **42**(18), 3694–3697 (2017).
18. J. C. Casals, S. Parsa, S. C. Kumar, K. Devi, P. G. Schunemann, and M. Ebrahim-Zadeh, "Picosecond difference-frequency-generation in orientation-patterned gallium phosphide," Opt. Express **25**(16), 19595–19602 (2017).
19. S. Guha, J. O. Barnes, and P. G. Schunemann, "Mid-wave infrared generation by difference frequency mixing of continuous wave lasers in orientation-patterned Gallium Phosphide," Opt. Mater. Express **5**(12), 2911–2923 (2015).
20. G. Insero, C. Clivati, D. D'Ambrosio, P. Natale, G. Santambrogio, P. G. Schunemann, J. J. Zondy, and S. Borri, "Difference frequency generation in the mid-infrared with orientation-patterned gallium phosphide crystals," Opt. Lett. **41**(21), 5114–5117 (2016).
21. M. R. Lorenz, G. D. Pettit, and R. C. Taylor, "Band gap of gallium phosphide from 0 to 900°K and light emission from diodes at high temperatures," Phys. Rev. **171**(3), 876–881 (1968).
22. A. L. Bajor, "Investigation of stress-induced birefringence in large semiconductor wafers by imaging polarimetry," Proc. SPIE **2265**, 431–442 (1994).
23. Y. Li, F. Liu, Y. Li, L. Chai, Q. Xing, M. Hu, and C. Wang, "Experimental study on GaP surface damage threshold induced by a high repetition rate femtosecond laser," Appl. Opt. **50**(13), 1958–1962 (2011).

1. Introduction

Coherent sources in the mid-infrared (mid-IR) spectral range are of great interest for a variety of scientific, industrial and medical applications [1–3]. Such applications continue to motivate the development of high-average-power mid-IR sources, particularly in the region of 2-10 μm. Numerous efforts have been directed towards the realization of such sources [4–6], with nonlinear optical techniques providing a particularly effective approach for practical generation of high-power and widely tunable mid-IR radiation. The advent of quasi-phase-matched (QPM) materials such as MgO-doped periodically-poled $LiNbO_3$ (MgO:PPLN) has heralded major breakthroughs in nonlinear frequency conversion technology. Today, optical parametric oscillators (OPOs) based on MgO:PPLN are firmly established as the most viable sources of widely tunable and high-power radiation in the 1-4 μm spectral range, limited by the onset of multi-phonon absorption in the oxide-based material above ~4 μm [7]. Therefore, the development of nonlinear frequency conversion sources at longer wavelengths into the deep mid-IR, offering practical performance, and in simple design, has remained challenging. As a result, access to the deep-IR spectral range has been most effectively achieved by exploiting nonlinear frequency conversion techniques based on non-oxide-based nonlinear crystals of oreintation-patterened GaAs (OP-GaAs) or $ZnGeP_2$ (ZGP) offering a long-wavelength absorption edge well beyond 4 μm. On the other hand, the short-wavelength absorption edge in OP-GaAs and ZGP at ~2 μm precludes the direct deployment of well-established solid-state or Yb-fiber lasers at ~1.06 μm, thus necessitating the use of cascaded OPO pumping [8], direct OPO pumping using Tm/Ho-doped solid-state lasers [9], or difference-frequency-generation (DFG) between Tm-fiber laser and OPO [10]. The choice of suitable materials offering the required linear and nonlinear optical properties, in addition to the short-wavelength transparency cut-off, are clearly key factors for practical and efficient frequency conversion. The efficiency of the frequency conversion process depends critically on several material parameters, including effective nonlinear coefficient (d_{eff}), type of interaction and polarization of the incident fields, as well as temperature and spectral phase-matching properties. Orientation-patterned gallium phosphide (OP-GaP) is the most recent non-oxide QPM semiconductor optical crystal, offering promising linear and nonlinear properties for deep mid-IR generation. It can potentially overcome several limitations of the

Optical Materials EXPRESS

established nonlinear materials such as $ZnGeP_2$ and OP-GaAs, which require pumping at wavelengths beyond ~2 μm [11]. OP-GaP exhibits higher thermal conductivity (110 W/m-K) and a larger bandgap (below ~1 μm), thus enabling near-IR to-deep-IR generation by deploying well-established pump laser technology at ~1.06 μm [12, 13]. However, during this early stage in the development of OP-GaP, several material properties still need to be studied and optimum growth parameters are yet to be established, in order to achieve the expected performance and realize the full potential of this crystal for nonlinear frequency conversion. Hence, it is imperative to perform detailed characterization of the linear and nonlinear optical properties of this material to evaluate its viability for nonlinear frequency conversion pumped at ~1.06 μm.

Over the past two years, there have been a number of reports on nonlinear frequency conversion in OP-GaP. These include a nanosecond OPO in doubly-resonant oscillator (DRO) configuration pumped at 1.064 μm, generating 4 mW of idler at 4624 nm and 15 mW of signal at 1324 nm at 10 kHz [14], as well as a nanosecond DRO pumped at 2.090 μm operating at a fixed idler wavelength of 5100 nm and a signal wavelength of 3540 nm, providing a total signal plus idler output power of 350 mW at 20 kHz [15]. Recently, we also demonstrated a tunable DFG source based on OP-GaP operating across 2548-2781 nm by mixing the input pulses from a Q-switched nanosecond Nd:YAG pump laser at 1.064 μm with the tunable signal from a MgO:PPLN pulsed OPO in a 40-mm-long crystal, providing up to ~14 mW of average output power at 80 kHz repetition rate [16]. In another report, we demonstrated an optical parametric generator (OPG) based on OP-GaP pumped directly by a Q-switched Nd:YAG laser at 1.064 μm [17]. The OPG was temperature-tuned across 1721-1850 nm in the signal and 2504-2787 nm in the idler, providing up to ~18 mW of the total average output power at 25 kHz repetition rate, with ~5 mW of the idler output power. Further, in the picosecond pulse regime, we demonstrated a single-pass DFG source by mixing the output signal of a picosecond OPO and ~20 ps pump pulses from a mode-locked Yb-fiber laser at 1.064 μm in OP-GaP, providing tunable DFG output across 3040-3132 nm with up to 57 mW of average power at 80 MHz repetition rate [18]. On the other hand, in the continuous-wave (cw) regime, single-pass DFG based on 16.5-mm-long OP-GaP crystal was reported, providing up to 150 mW of output power at a fixed wavelength of 3400 nm for an input pump power of 47 W at 1.064 μm, together with 24 W of signal power at 1550 nm [19]. Recently using a 24.6-mm-long OP-GaP crystal, a cw DFG power of 65 μW was generated at a fixed wavelength of 5850 nm for a pump power of 10 W at 1.064 μm and a signal power of 40 mW at 1301 nm [20].

In this work, we report a systematic performance characterization of tunable single-pass mid-IR DFG in OP-GaP, for the first time. Using a 40-mm-long OP-GaP crystal, we have investigated several important parameters including parasitic wavelength generation, mid-IR DFG tuning, power scaling, temperature as well as spectral acceptance bandwidths. We have also studied the dependence of DFG power on the polarization of the incident fields, performed transmission measurements at the pump and signal wavelength, and investigated thermal effects and damage threshold limitation of the OP-GaP sample.

2. Experimental setup

The schematic of the experimental setup for single-pass DFG in OP-GaP is similar to that described in Ref [16]. The input pump source is a Q-switched Nd:YAG laser (*Bright Solutions, Sol*), delivering up to 30 W of average power at ~1064 nm in linear polarization, with a tunable repetition rate of 20-100 kHz. The output pulse duration varies from ~8 ns at 20 kHz to ~26 ns at 100 kHz repetition rate. However, for the experiments presented in this report, we used a repetition rate of 80 kHz, resulting in a pump pulse duration of ~23 ns. The instantaneous bandwidth and frequency jitter of this laser are measured to be <0.5 nm and ~1 nm over 0.5 minutes, respectively. A major portion of the output power from the laser is used to pump a pulsed OPO, which provides the input signal beam for DFG in the OP-GaP

Optical Materials EXPRESS

crystal, while the remaining power is used as the pump for the DFG process. The nonlinear gain medium for the pulsed OPO is a 38-mm-long, 1-mm-thick MgO:PPLN crystal with five grating periods ranging from Λ_{OPO}=29.5 to 31.5 μm in steps of 0.5 μm. However, in the present experiments, we used a single grating period of Λ_{OPO}=31.5 μm. The end faces of the crystal are antireflection (AR)-coated for the pump and idler (R<4%), with high transmission (R<1%) for the signal over 1300-1900 nm. The crystal is housed in an oven, which can be adjusted from room temperature to 200 °C with a stability of ±0.1 °C. The OPO is configured as a singly-resonant oscillator (SRO) for the signal in a three-mirror cavity arrangement. In order to partially extract the signal from the OPO, we use a ~22% output coupler, while the idler is extracted in single-pass through the cavity and filtered from the pump. For the fixed grating period of Λ_{OPO}=31.5 μm, the OPO can be temperature-tuned over 1664-1928 nm in the signal and 2374-2950 nm in the idler. The signal from the OPO and the remaining pump from the laser are collimated and combined using a dichroic mirror, which is coated for high reflectivity (R>99%) for the signal over 1300-2000 nm and high transmission (T>90%) for the pump at 1064 nm. The pump and signal beams are focused to waist radius of w_{op}~65 μm and w_{os}~60 μm, respectively, at the center of the OP-GaP crystal. These focal spots correspond to focusing parameter of ξ_p~0.5 and ξ_s~1 for the pump and signal, respectively. The nonlinear crystal for DFG is a 40-mm-long OP-GaP sample, which is 6-mm-wide, 1.7-mm-thick, and contains a single grating period of Λ_{DFG}=15.5 μm. The resulting DFG beam waist in the OP-GaP crystal is estimated to be w_{oi}~44 μm, with a corresponding focusing parameter of ξ_i~2.6. The crystal end-faces are AR-coated for high transmission (R<1%) at 1064 nm and 1500–1900 nm, with >80% transmission over 2500-2800 nm. The DFG output is extracted after separation from the pump and signal using a Ge filter, and measured using a power meter.

3. Parasitic processes

Initially, with the input pump beam incident on the OP-GaP sample, we observed weak green light generation through non-phase-matched frequency doubling of the pump light. By careful alignment of both pump and signal beams through the crystal, a parasitic output beam in the red could also be observed. A typical spectrum of the parasitic red light at 664.6 nm, measured using a visible spectrometer (*Ocean Optics*, HR4000), obtained at an OP-GaP crystal temperature of 115 °C, is shown in Fig. 1(a). Here the spectral intensity is not to scale. The measured spectrum corresponds to higher-order QPM sum-frequency-generation (SFG) of the pump at 1064 nm and signal at 1770 nm. We also detected another parasitic component at 761.4 nm resulting from SFG between the DFG output and the pump, as can also be seen in Fig. 1(a), as well as a weak frequency doubling of the signal beam at 885 nm. The total average power in the parasitic components was measured to be <1 mW, compared to the DFG output power of ~14 mW. Also shown in the inset of Fig. 1(a) is the parasitic SFG output in the red produced by the 40-mm-long OP-GaP crystal during the DFG process. We estimated the QPM grating periods required to generate the parasitic light using the relevant temperature-dependent Sellmeier equations [14]. The calculation resulted in a grating period of Λ_{SFG}~3.4 μm for the SFG between pump and signal, Λ_{SFG}~6.2 μm for the SFG between the pump and DFG output. The DFG tuning was achieved by simultaneously varying the OPO signal wavelength and the phase-matching temperature of the OP-GaP crystal. The corresponding parasitic wavelength tuning as a function of the OP-GaP crystal temperature is shown in Fig. 1(b). For a fixed pump wavelength of 1064 nm, varying the signal wavelength across 1723-1827 nm together with OP-GaP crystal temperature over 50-150 °C, resulted in a parasitic SFG tuning over 658-672 nm (pump + signal) and 770-753 nm (pump + DFG). The hollow and filled circles in Fig. 1(b) correspond to the measured parasitic SFG wavelength data. The solid lines are theoretical calculations using the relevant Sellmeier equations for OP-GaP [14]. In the calculations, the value of the OP-GaP grating period was optimized to Λ=15.56 μm, in order to obtain the best match to the experimentally measured SFG

Optical Materials EXPRESS

wavelengths. From the measured SFG data, we deduced an experimental DFG tuning range from 2548 to 2781 nm (233 nm), while the theoretical DFG tuning range was calculated to be from 2492 to 2782 nm (290 nm), as presented in the inset of Fig. 1(b). Hence, there is good agreement between the experimental tuning range deduced from the parasitic SFG tuning data and theoretical tuning range based on a grating period of Λ=15.56 μm. Across the DFG tuning range, we generated >6 mW of average output power.

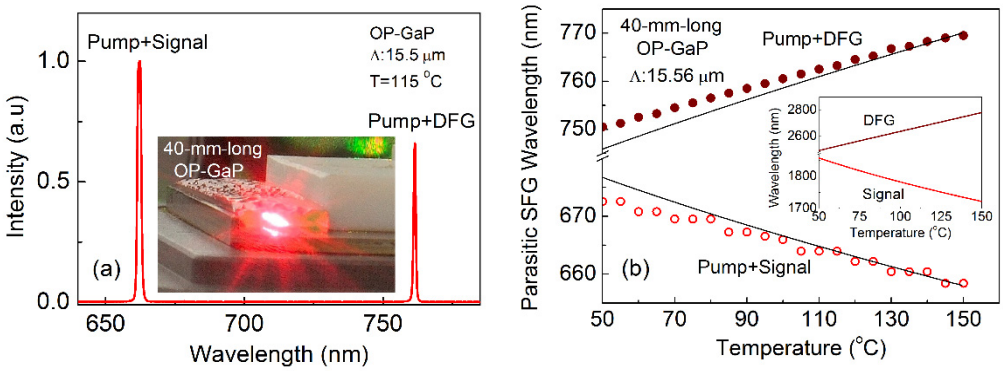

Fig. 1. (a) Spectrum of the generated parasitic SFG at 664.6 nm (pump + signal) and at 761.4 nm (pump + DFG). Inset: 40-mm-long OP-GaP sample generating red parasitic output beam at the exit of the crystal. (b) Variation of the parasitic SFG wavelengths as a function of OP-GaP crystal temperature. Inset: Corresponding DFG temperature tuning.

4. Temperature acceptance bandwidth

In order to study the phase-matching properties of the 40-mm-long OP-GaP crystal for the DFG process, we performed temperature acceptance bandwidth measurements. We used the same focusing condition as for DFG, with w_{op}~65 μm and w_{os}~60 μm, corresponding to focusing parameter of ξ_p~0.5 and ξ_s~1 for the pump and signal, respectively, at the center of the OP-GaP crystal. For these measurements, the pump and signal polarizations were arranged as $\psi_p=\psi_s=54.7°$ (see Section 6), and the pump and signal powers were maintained constant at 3 W and 0.6 W, respectively. For a pump wavelength of 1064 nm and a fixed signal wavelength of 1766 nm, generating a DFG wavelength of 2676 nm, the normalized DFG power as a function of the temperature deviation about the phase-matching temperature is shown in Fig. 2(a). Also shown is the $sinc^2$ fit to the experimental data, resulting in a full-width at half-maximum (FWHM) temperature acceptance bandwidth of ΔT~18 °C, centered at ~103 °C. The theoretically calculated temperature acceptance bandwidth for a 40-mm-long OP-GaP crystal with a grating period of Λ=15.56 μm, using the temperature-dependent Sellmeier equations [14], is shown in Fig. 2(b). As can be seen, the experimentally measured bandwidth is substantially larger than the theoretical FWHM value of ΔT~1 °C. It is also to be noted that the theoretically calculated phase-matching temperature of ~113.2 °C is significantly different from the measured value of 103.3 °C. However, it is closer to the measured experimental value than the estimated value for an OP-GaP crystal with a grating period of Λ=15.5 μm, which is calculated to be 124.4 °C. The large discrepancy in the phase-matching temperature and acceptance bandwidth could be attributed to the uncertainty in the grating period, wide spectral bandwidth of pump and signal beams, linear absorption losses as well as thermal effects due to absorption in the crystal. In addition, the calculation of acceptance bandwidth is based on plane-wave approximation, while the experimental measurements correspond to focused beams, which were necessary, given the restricted useful aperture of the grating region and the limited DFG efficiency due to crystal absorption (see Section 8).

Optical Materials EXPRESS

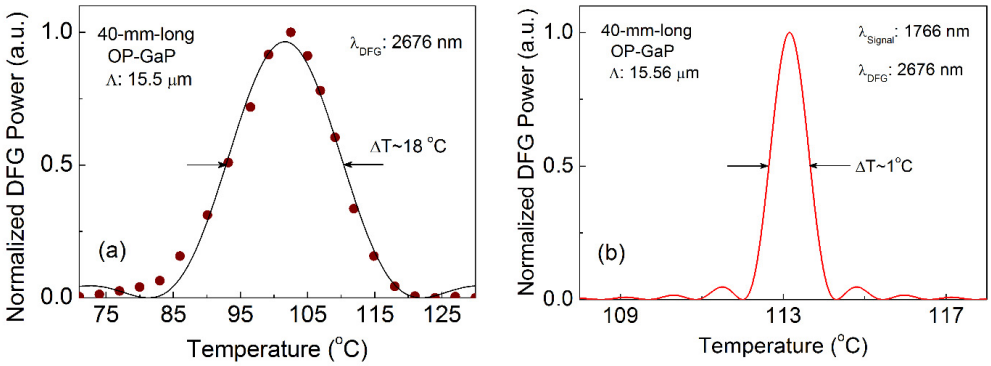

Fig. 2. (a) Experimentally measured temperature acceptance and the corresponding *sinc*^{2} fit, and (b) theoretically calculated temperature acceptance bandwidth, for the 40-mm-long OP-GaP crystal.

5. Spectral acceptance bandwidth

We further investigated the spectral acceptance bandwidth of the 40-mm-long OP-GaP crystal. The normalized DFG power as a function of the signal wavelength, for a fixed pump wavelength, is shown in Fig. 3(a). For this measurement, the phase-matching temperature was optimized for every signal wavelength to achieve maximum DFG power. Also shown in Fig. 3(a) is the *sinc*^{2} fit to the experimental data, resulting in a FWHM acceptance bandwidth of $\Delta\lambda_{signal}$~17 nm. This is also much wider than the theoretically estimated spectral acceptance bandwidth of $\Delta\lambda_{signal}$~4 nm for a 40-mm-long OP-GaP crystal at wavelength of 1760 nm using the temperature-dependent Sellmeier equations for the material [14]. It is also to be noted that the theoretically calculated phase-matching temperature for an OP-GaP grating period of Λ=15.5 μm is ~129 °C, which is much higher than the measured experimental value 103.3 °C. On the other hand, the phase-matching temperature calculated for the grating period of Λ=15.56 μm is 122 °C, as shown in Fig. 3(b), indicating that the difference in the phase-matching temperature is caused by the uncertainty in the grating period. Other factors contributing to the discrepancy include linear absorption losses, additional thermal effects due to crystal absorption, and broad bandwidth of the input pump and signal pulses used in the DFG experiment.

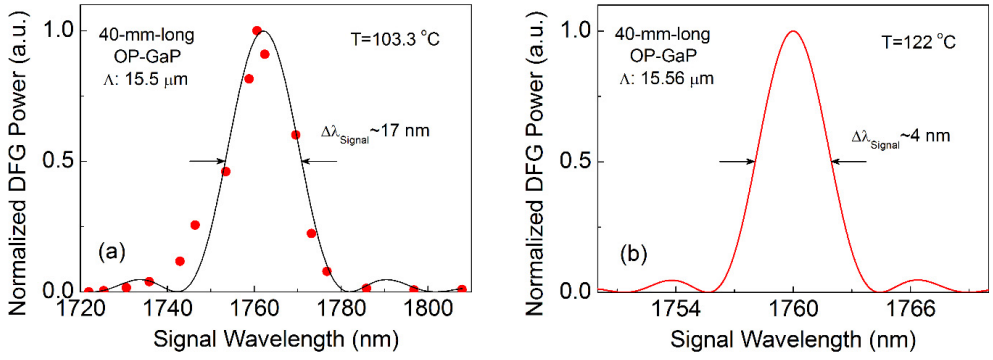

Fig. 3. (a) Experimentally measured spectral acceptance and the corresponding *sinc*^{2} fit, and (b) theoretically calculated spectral acceptance bandwidth for the 40-mm-long OP-GaP crystal.

6. Polarization dependence and optimization

Gallium phosphide is a cubic nonlinear material, and due to the high symmetry, birefringent phase-matching is not available, so that all nonlinear optical processes are achieved by QPM

Optical Materials EXPRESS

interaction through orientation-patterning [14]. Therefore, several different polarization combinations can provide access to nonlinearity. As such, both linear and circularly polarized light have been used to realize nonlinear frequency conversion in OP-GaP [19]. However, in order to achieve maximum conversion efficiency in OP-GaP, the pump and signal beams should be linearly polarized. Hence, it is important to optimize the polarization of the incident input beams independently, thereby accessing the maximum nonlinear gain coefficient in the crystal. The polarization-dependent gain factor, δ^2, which is defined as the ratio of the effective nonlinear coefficient to d_{14} for linearly polarized incident beams in OP-GaP is given by [19]

$$\delta^2 = \left(\frac{d_{eff}}{d_{14}}\right)^2 = \sin^2\left(\psi_p + \psi_s\right) + \sin^2\psi_p \sin^2\psi_s$$

Here, ψ_p and ψ_s represent the angle between the pump and signal polarization vectors relative to the [100] plane in the OP-GaP crystal, respectively. The variation of the gain factor, δ^2, as a function of pump and signal polarizations is shown in the Fig. 4(a). As can be seen, for a pump polarization parallel to the [100] plane (ψ_p=0°), the gain factor varies sinusoidally as a function of signal polarization (ψ_s), reaching maximum of δ^2=1. However, for the pump polarization perpendicular to the [100] plane (ψ_p=90°), δ^2 remains constant at unity, accessing a nonlinear coefficient of d_{14}, irrespective of the signal polarization (ψ_s). However, a maximum nonlinear coefficient of 1.3 times d_{14} can be achieved by arranging both the pump and signal polarization directions along the base diagonal (ψ_p=ψ_s=54.7°) in the first quadrant. Other ($\psi_{p,s}$) combinations resulting in maximum δ^2=1.3d_{14} also exist in the second, third, and fourth quadrant. Figure 4(b) further illustrates the maximum and minimum values of the gain factor that can be achieved for different pump polarizations, while scanning the signal polarization. It can be seen that frequency conversion can always be realized with a non-zero value of δ^2, for any ψ_s with ψ_p>0°.

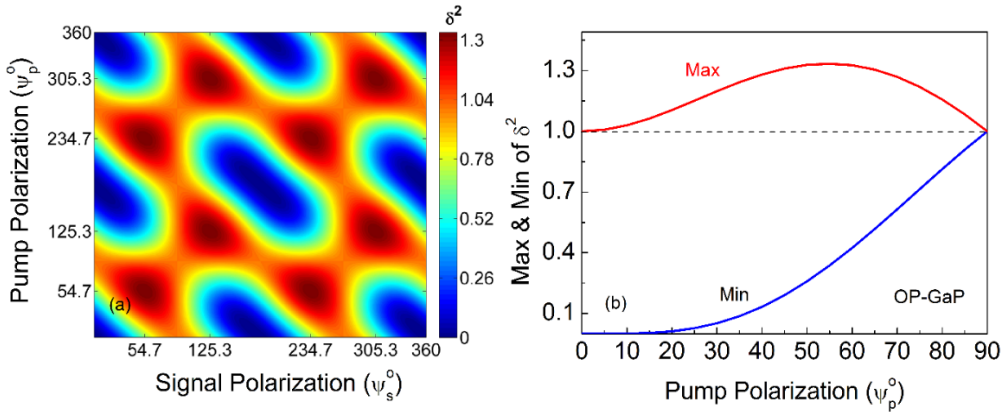

Fig. 4. (a) Variation of the nonlinear gain factor (δ^2) as function of the pump and signal polarization in OP-GaP. (b) Variation of the maximum and minimum values of the gain factor for different pump polarizations in the first quadrant.

Optical Materials EXPRESS

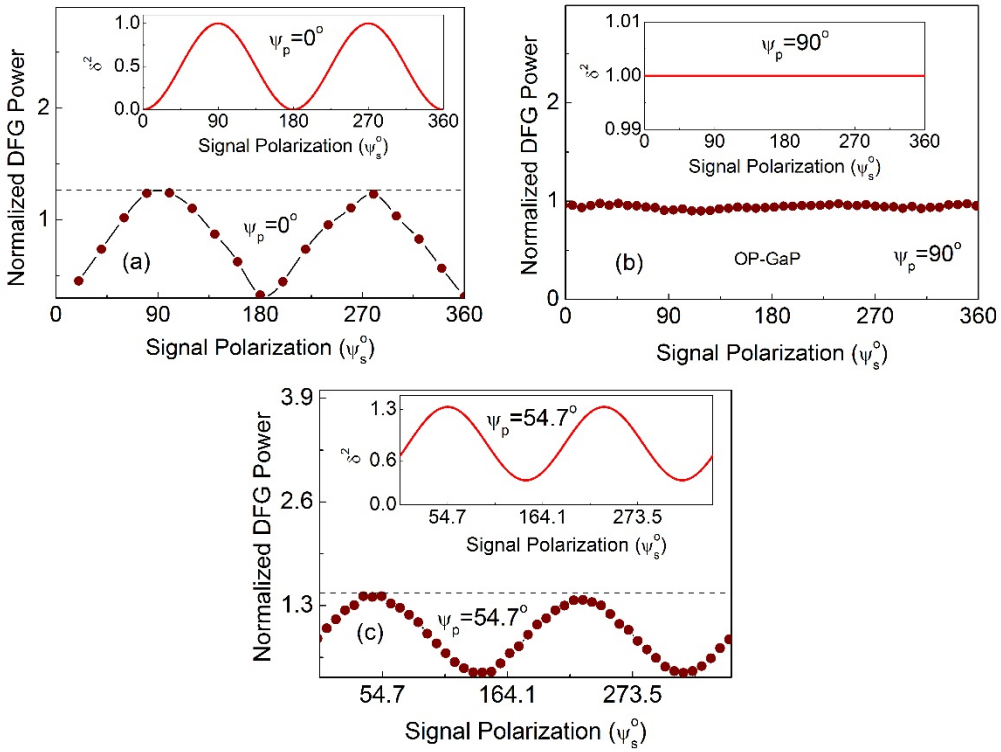

Fig. 5. Variation of the normalized DFG output power as a function of signal polarization, ψ_s, for a fixed pump polarization of (a) ψ_p=0°, (b) ψ_p=90°, (c) ψ_p=54.7°. Inset: Corresponding theoretical calculations.

In order to study the dependence of the frequency conversion process on the incident beam polarizations in OP-GaP, we measured the DFG output power, which is proportional to δ^2, for three different pump polarizations, while varying the input signal polarization. The results are presented in Fig. 5(a-c). Two independent half-wave plates were used to vary the pump and signal polarizations and the measured DFG power was normalized with respect to that for ψ_p=90° (δ^2=1). The corresponding theoretical calculations showing the variation of δ^2 as a function of signal polarization (ψ_s) for the three different pump polarizations (ψ_p) are also presented in the insets of Fig. 5(a-c). For a fixed pump polarization of ψ_p=0°, with a constant power of 3 W at 1064 nm and a signal power of 0.6 W at 1748 nm, the variation of the normalized DFG power as a function of signal polarization is shown in Fig. 5(a). As predicted, the normalized DFG power varies sinusoidally with signal polarization, with a minimum at ψ_s=0°, while reaching a maximum of ~1.2 at ψ_s=90°, which is close to the theoretical value of 1. Similar measurements for the orthogonal pump polarization of ψ_p=90° resulted in a constant output as a function of signal polarization, as shown in Fig. 5(b), as expected. Moreover, as evident from Fig. 5(c), when the pump polarization is fixed at ψ_p~54.7°, the normalized DFG power again varies sinusoidally, reaching a maximum of ~1.4 for a signal polarization of ψ_s~54.7°. This value is again close the theoretically predicted value of 1.3.

7. Power scaling

We also performed power scaling measurements by recording the variation of DFG output power as a function of input pump power for two different pump polarization angles of ψ_p=54.7° and ψ_p=90°, with the results shown in Fig. 6. The signal average power and polarization were fixed at 1 W and ψ_s=54.7°, respectively, while operating at 1748 nm and a

Optical Materials EXPRESS

phase-matching temperature of 123.7 °C, resulting in a DFG wavelength of 2719 nm. For each pump polarization, the signal polarization was optimized to achieve maximum DFG output power. As evident from Fig. 6, the DFG power increases linearly as function of pump power, generating as much as 14 mW (ψ_p=54.7°) and 9 mW (ψ_p=90°) for a maximum pump power of 5 W, resulting in a DFG power ratio of ~1.5 for the two pump polarizations, slightly higher than the expected values of 1.3. The corresponding slope efficiencies are estimated to be 0.3% and 0.15%, respectively. The discrepancy in the attainable maximum power could be attributed to inhomogeneity in the transmission leading to absorption in our OP-GaP crystal at the pump, signal and DFG wavelengths, which are in turn dependent on polarization and temperature, as discussed in Section 8. While performing the power scaling measurements, the temperature of OP-GaP crystal was optimized for each pump power to achieve the maximum DFG output power. As the pump power was increased from 0.6 W to 5 W, the phase-matching temperature of the OP-GaP had to be reduced by ~30 °C, indicating strong thermal effects. This change in temperature is much greater than the measured temperature acceptance bandwidth of 18 °C presented in Fig. 2, and can be attributed to the absorption at the pump and signal wavelengths, resulting in the temperature rise in the OP-GaP crystal, thereby necessitating the reduction of the phase-matching temperature. We measured the transmission for the pump and signal beams, while producing the maximum DFG power of 14 mW, and found them to be 28% and 18%, respectively. Taking into account the losses in the OP-GaP crystal, the generated maximum DFG power represents a pump-to-DFG conversion efficiency of ~1%, corresponding to a photon conversion efficiency of ~2.5%. A similar measurement for a fixed pump power of 5 W resulted in a maximum DFG power 14 mW at a slope efficiency of 1.2% with respect to the signal power. It is to be noted that the DFG powers presented here are not corrected for the losses in the crystal and the separation filters used in the experiment. Also shown in the inset of Fig. 6 is the spatial quality of the DFG output beam recorded using mid-IR beam profiler, while generating maximum power. The measurement confirms a high beam quality with single-peak Gaussian intensity distribution. Further, the passive power stability of the DFG power was also recorded at 2774 nm and found to be better than 1.7% rms over 1.4 hours.

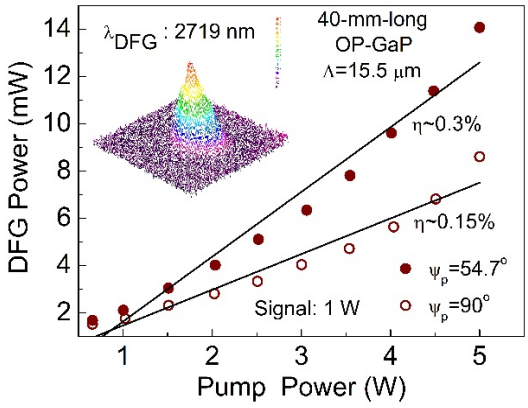

Fig. 6. DFG power scaling as a function of the pump power at a constant signal power for two different pump polarizations of ψ_p=54.7° and ψ_p=90°. Inset: Spatial beam profile of the DFG beam at maximum power.

Optical Materials EXPRESS

8. Transmission

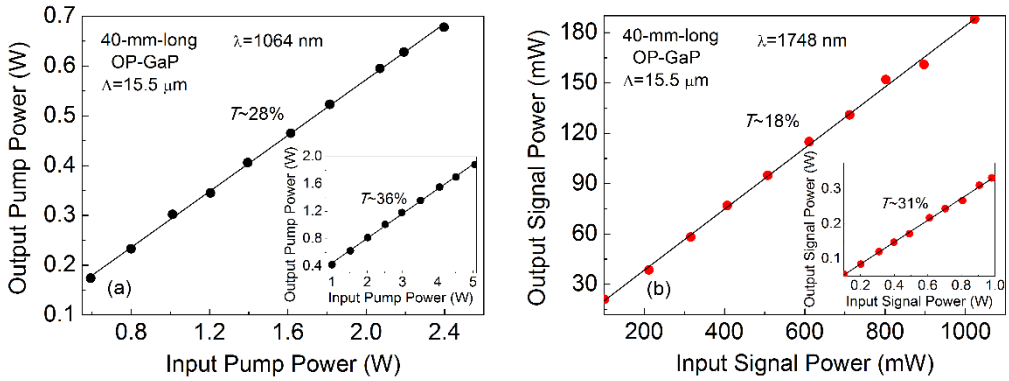

Fig. 7. Transmission measurements of the 40-mm-long OP-GaP crystal at room temperature for (a) pump, and (b) signal wavelengths, while generating a maximum DFG power at 2719 nm. Inset: Similar measurements at a different position in the crystal.

In order to study thermal effects in the OP-GaP crystal during the DFG process, we performed transmission measurements at the pump and signal wavelengths. With the pump and signal polarization set to $\psi_p=\psi_s=54.7°$ and generating the maximum DFG power at 2719 nm, and the crystal operating near room temperature (T~28 °C), we measured a transmission of 28% at the pump wavelength of 1064 nm and 18% at a signal wavelength of 1748 nm. The results are shown in Fig. 7(a,b). Similar measurements at a different position in the OP-GaP crystal are presented in the inset of Fig. 7(a,b), showing higher transmission of 36% and 31% for the pump and signal, respectively, without significant improvement in the DFG output power. This indicates inhomogeneous transmission through the crystal and non-uniformity in the grating period. Using the data obtained from the transmission measurements, we estimated the losses at the pump and signal wavelengths at each of the two positions in the OP-GaP crystal to be α_{Pump}~32 m^{-1} and α_{Signal}~43 m^{-1} at position 1 [Fig. 7(a,b)], and α_{Pump}~26 m^{-1} and α_{Signal}~29 m^{-1} at position 2 [inset, Fig. 7 (a,b)]. Since the OP-GaP crystal end-faces are AR-coated for high transmission (R<1%) at 1064 nm and 1500–1900 nm, with >80% transmission over 2500-2800 nm, the major contribution to the drop in the transmission at the interacting wavelengths is associated with the absorption and propagation losses in the bulk crystal. We also observed that the transmission of the crystal was dependent on the operating temperature, as reported previously [17,21]. The low crystal quality, operating at a pump wavelength close to the band edge and the temperature dependence of the absorption could be attributed to the Urbach tail or free-carrier absorption in OP-GaP. To gain further insight, we also investigated the transmission of the OP-GaP crystal at 1064 nm under irradiation in other time-scales, by deploying a continuous-wave (cw) as well as a high-repetition-rate picosecond Yb-fiber laser at 80 MHz, in addition to the nanosecond pulses. During the systematic characterization, we ensured the use of the same position in the crystal and an identical maximum average pump power of 5 W for all the measurements. The laser beam in all three cases was also focused to a beam waist radius of w_{op}~90 μm inside the crystal. The measured transmission of the crystal as a function of temperature for the two orthogonal pump polarizations at 1064 nm is as shown in Fig. 8(a-c).

Optical Materials EXPRESS

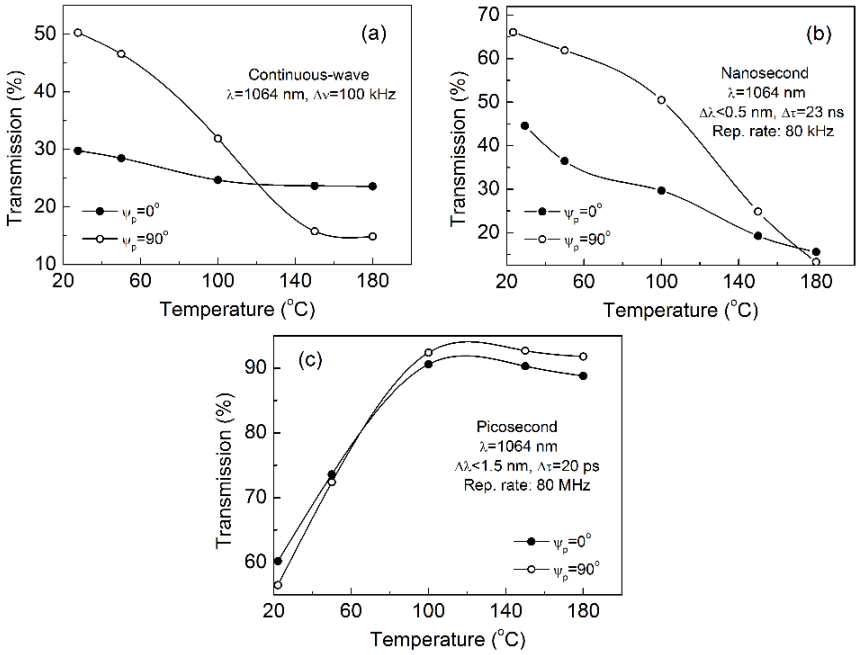

Fig. 8. Transmission of the 40-mm-long OP-GaP crystal at 1064 nm in (a) continuous-wave, (b) nanosecond, and (c) high-repetition-rate picosecond time-scale, for the two orthogonal pump polarizations.

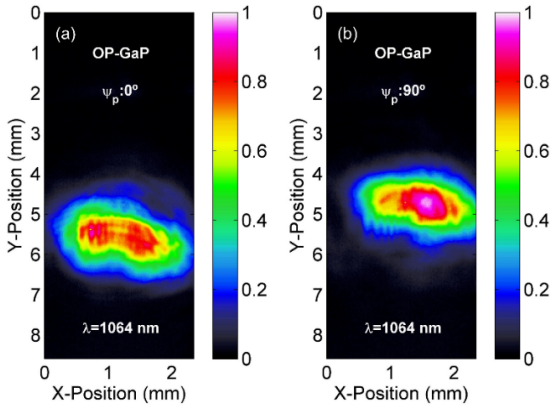

Fig. 9. (Visualization 1) The shift in the spatial position of the pump beam at 1064 nm as function of polarization. (a) ψ_p=0°, (b) ψ_p=90°.

As evident, the transmission is observed to decrease significantly with increase in temperature in the cw as well as nanosecond time-scale, while it is recorded to increase in the picosecond regime. We do not currently have an explanation for this behavior, and further studies are necessary to identify the underlying mechanisms responsible for the transmission properties of the OP-GaP crystal under irradiation in different time-scales. During these transmission measurements, we also observed a shift in the pump beam as a function of polarization as presented in Fig. 9, Visualization 1. In this case, the nanosecond pump beam was focused using a f=250 mm focal length lens in the OP-GaP crystal and the transmitted beam was monitored at distance of 18 cm from the exit face of the crystal using a beam profiler. As the pump beam polarization was varied from ψ_p=0 to 90°, the transmitted beam was observed to shift by ~1 mm in the vertical plane, as presented in the Media file. This

Optical Materials EXPRESS

polarization-dependent beam walkoff could be attributed to stress-induced birefringence during the growth process of the OP-GaP crystal [22] or lattice-mismatch-induced strain, leading to thermal anisotropy and refractive index distribution, which is in turn dependent on the polarization. All these measurements indicate the poor quality of this first 40-mm-long OP-GaP crystal sample used in our experiments in terms of the transmission and grating uniformity.

9. Thermal effects and damage limitations

The low transmission at the pump and signal wavelengths immediately suggests significant thermal effects in the OP-GaP crystal. Hence, we performed systematic measurements to estimate the temperature rise on the surface of the crystal using a point-contact thermocouple. As the pump power at the input to the OP-GaP crystal was increased to a maximum of 5 W, with no input signal, we measured a temperature rise as high as ~17 °C. However, when the incident signal power was increased to 1 W, with no input pump, the temperature rise was recorded to be only about 4.5 °C. On the other hand, while generating the maximum DFG power of 14 mW, with 5 W of pump and 1 W signal power at the input to the OP-GaP crystal, the temperature rise on the surface of the crystal was as high as ~20 °C. Further, we observed that the time required to reach the maximum DFG power was longer for an incident pump power of 5 W with fixed input signal power than that required when the pump power was fixed with an incident signal power of 1 W. When the signal power was fixed, the crystal reached a steady-state temperature, and releasing the pump power led to a large temperature rise. Hence, the crystal required longer time to reach the final steady-state phase-matching temperature. These measurements indicate that the absorption at the pump wavelength is much more significant than at the signal and DFG wavelengths. Such high absorption at the pump wavelength could eventually lead to damage in the OP-GaP crystal. Hence, we also attempted to characterize the OP-GaP crystal for damage at the 1064 nm. The pump beam, with polarization set to ψ_p=54.7°, was focused to a waist radius of w_{op}~75 μm inside the crystal at room temperature. The maximum tolerable average power before the observation of bulk damage in the OP-GaP crystal, and the corresponding peak pulse intensity, as function of the pump laser repetition rate, are shown in Fig. 10(a). As can be seen, the maximum power before the crystal experiences damage increases linearly from 1.8 W at 20 kHz to 12 W at 80 kHz. It is to be noted that the pulse duration also varies from 8 ns at 20 kHz to 23 ns at 80 kHz, which is also accounted for in the calculated peak intensity. The variation of the corresponding pulse energy and the fluence is shown in Fig. 10(b), where it can be seen that at repetition rates >40 kHz, the pulse energy fluence is clearly the limiting factor, resulting in a damage threshold of ~0.84 J/cm^2. However, at lower repetition rates <20 kHz, the damage is observed to occur at a peak intensity of 62 kW/cm^2, corresponding to an energy fluence of 0.5 J/cm^2, due to the relatively short pulse duration. Owing to low transmission of our OP-GaP sample at the pump wavelength, this damage threshold is ~6.4 times lower than that reported in the literature for the crystal [23]. However, no surface damage was observed during these measurements.

Optical Materials EXPRESS

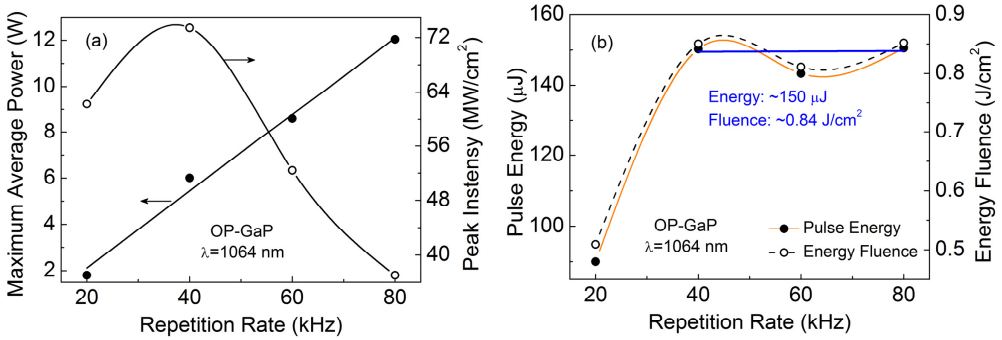

Fig. 10. (a) Maximum tolerable average pump power before damage in the OP-GaP crystal, and the corresponding peak intensity. (b) Pulse energy and fluence, as a function of the pump laser repetition rate at 1064 nm.

10. Conclusions

In conclusion, we have reported a systematic study on the performance characteristics of tunable pulsed nanosecond DFG in the new semiconductor nonlinear material, OP-GaP. The DFG source has been realized by single-pass mixing of a Q-switched Nd:YAG laser at 1064 nm with the output signal beam from a pulsed OPO based on MgO:PPLN in OP-GaP. We have generated up to ~14 mW of DFG average power at 2719 nm at 80 kHz repetition rate, with >6 mW across the full tuning range of 2548-2781 nm, in TEM_{00} spatial profile. The temperature and spectral acceptance bandwidths for the DFG process in the 40-mm-long OP-GaP sample have been measured to be ΔT~18 °C and $\Delta\lambda_{signal}$~17 nm, respectively. The corresponding theoretical calculations indicate some discrepancy due to the uncertainty and possible non-uniformity in the grating period, as well as thermal effects due to crystal absorption. Further, we have also performed detailed characterization of the nonlinear gain for DFG and its dependence on the polarization of incident pump and signal fields. These measurements have resulted in the achievement of maximum DFG power when the incident beams are polarized along the body diagonal, in good agreement with theory. The transmission measurements of the OP-GaP crystal at the pump and signal wavelengths provide understanding about the DFG efficiency. Further, the transmission at the pump and signal wavelengths has been found to be dependent on spatial position, temperature, as well as polarization. Moreover, temperature dependence of the transmission in OP-GaP has been investigated in cw, nanosecond, as well as picosecond time-scales. The transmission is found to reduce with temperature in the cw and nanosecond time-scales, while it is found to be improved at high temperatures in the picosecond regime. Detrimental thermal effects were studied by recording the increase in the surface temperature of our OP-GaP crystal. By exploiting the repetition-rate tunability of our nanosecond pump laser, we have estimated the damage threshold of the OP-GaP sample to be ~0.84 J/cm^2. To the best of our knowledge, this is the first report on detailed characterization of the OP-GaP crystal for pulsed DFG. We believe, with further progress in the growth of OP-GaP crystals with higher transmission and improved QPM grating quality in terms of uniformity and aperture, substantial improvements in the efficiency, output power, and beam quality will be attainable, enabling OP-GaP to fully realize its potential as a viable and promising new nonlinear crystal for mid-IR frequency conversion applications.

Funding

Ministerio de Economía y Competitividad (MINECO) (nuOPO, TEC2015-68234-R); European Commission (Mid-Tech, H2020-MSCA-ITN-2014); Severo Ochoa Programme for Centres of Excellence in R&D (SEV-2015-0522); CERCA Programme/Generalitat de Catalunya; Fundación Cellex.